Numerical simulation of the stress field in California: implications for the stress perturbation by Big Bend and Garlock Fault

M. P. KOIRALA* AND D. HAYASHI

Simulation Tectonics Laboratory, Faculty of Science, University of the Ryukyus, Okinawa, 903-0213, Japan.

**e-mail: matrikakoirala@gmail.com*

Abstract: 2D finite element modelling is used to analyze the state of stress in and around the San Andreas Fault System (SAFS) taking the whole area of California. In this study we focus on the state of stress at the general seismogenic depth of 12 km, imposing elastic rheology. The purpose of the present study is to simulate the regional stress field and also to find the stress perturbation due to Big Bend and Garlock Fault. Although in nature there is lateral and vertical variation in rheology, our highly simplified domain properties have simulated results comparable with the observed data. Our imposed boundary condition (fixed North American plate, Pacific plate motion along N34W vector up to northern terminus of the San Andreas faults and N50E vector motion for the subducting Gorda plate) simulated the present day regional $_{Hmax}$ orientation and velocity vector. Simulated results show local effect on the stress field and displacement vector by the Big Bend and is further enhanced by the Garlock Fault, which may have significant impact on fault slip, stress, and hence deformation in the surrounding region.

Keywords: San Andreas Fault System (SAFS), 2D finite element modelling, Big Bend, Garlock Fault, σ_{Hmax}, velocity vector.

The San Andreas Fault System (SAFS), a complex system of faults that display predominantly large-scale strike slip displacement, is part of an even more complex system of faults, isolated segments of the East Pacific Rise, and scraps of plates lying east of the East Pacific Rise that collectively separate the North American plate from the Pacific plate (Wallace, 1990). The SAFS is mainly a right-lateral strike slip fault. It has many other small faults, some are left-lateral, some are thrusts and some normal faults. Present-day plate kinematics of the Pacific and North American plates reveals that the Pacific plate is moving towards NW with respect to North American plate. The motion of the plate is approximately 3.4-6 cm a[-1] on a N34W vector approximately (Atwater, 1970; Minster and Jordan, 1978; DeMets *et al.*, 1994; Argus and Gordon, 2001; Savage *et al.*, 2004; d'Alessio *et al.*, 2005). At its north end, the San Andreas Fault joins the Mendocino Fracture Zone at a high angle, and there the Gorda plate and Juan de Fuca plate are being subducted under the North American plate. The Juan de Fuca plate currently subducts under the North American plate with a generalized vector motion of N50E (Swanson *et al.*, 1989) and with a velocity of 3 cm a[-1] (Noson *et al.*, 1988). The Gorda plate subducts with a similar direction, but at an average velocity of 1.8 cm a[-1] (Wood and Kienle, 1990). Generally, it is said that the SAFS is a fault oblique to the compression direction. However, it is not so simple, if it is considered that in the area very near to the main fault the state of stress is fault oblique compression and away from the fault the state of stress is fault perpendicular compression (as shown by fold axes parallel to the fault strike). It also depends on the depth where we are measuring the maximum horizontal stress. In the present study,
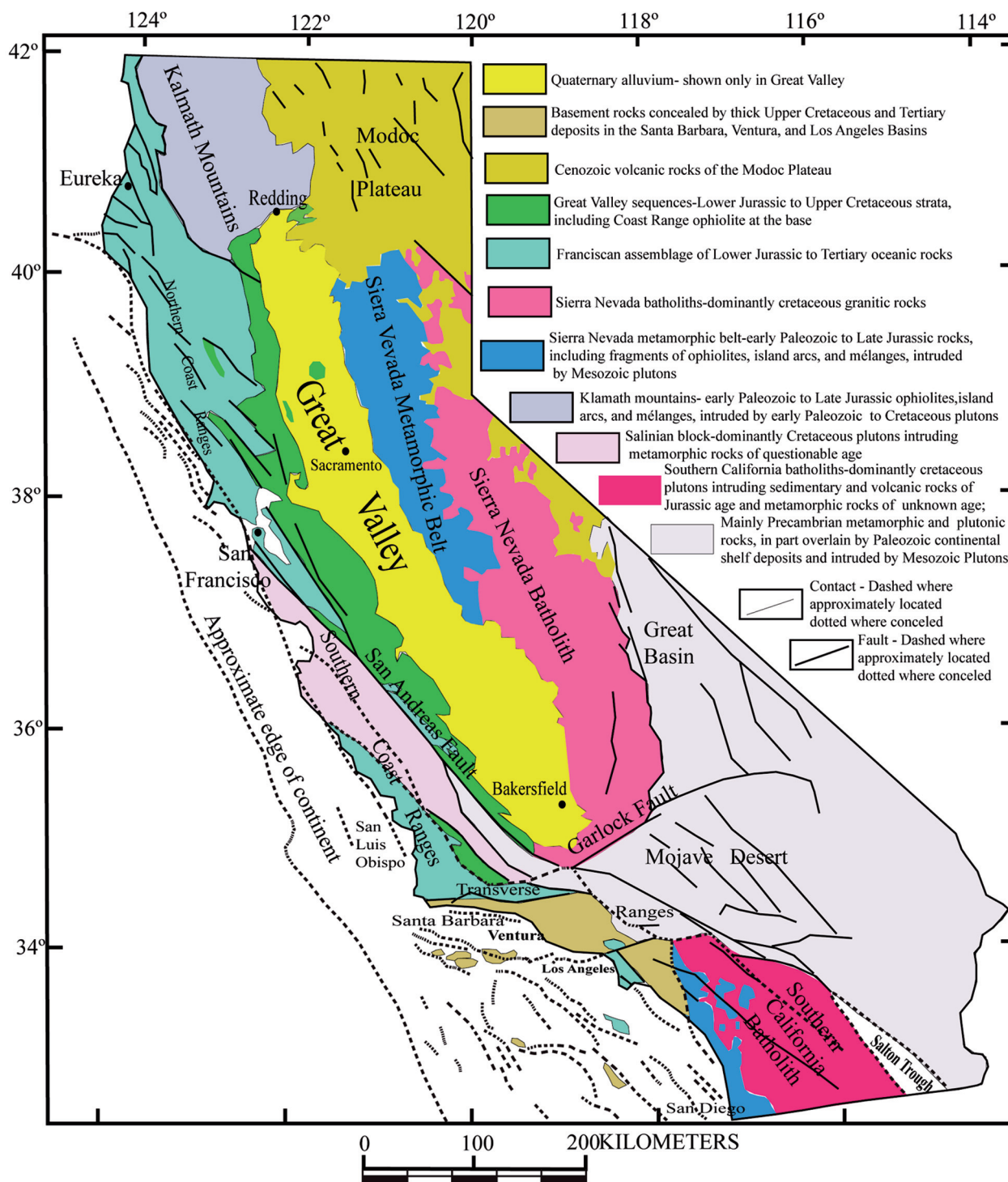
Figure 1. Simplified geological map of California (modified after Irwin, 1990 and references therein).

we calculated the stress at the seismogenic crust (at 12 km depth) of the whole California area and tried to analyze the effect of the Big Bend and Garlock Fault on the stress field and displacement vector. For this, we use simple but powerful FE plain stress modelling.

The objectives of the present study are: 1) evaluate the state of stress along and around the SAFS, California; 2) decipher the stress perturbations due to the big bend and Garlock Fault on the SAFS; and 3) unravel the deflection in displacement vector by the Big Bend and Garlock Fault.

Elastic plane stress FE models are created to analyze the state of the stress on the whole California region, especially along and around the SAFS (Hayashi, 2008). Different domains are created in the model through variation of the domain properties. The simplified geological map of California modified after Irwin (1990) is taken as the base map (Fig. 1).

Model description

Models are created to analyze the state of stress along and around the SAFS. The simplified geological map of California (Fig. 1) is taken as the base map.

The FE software has been used in order to solve the elastic equations and for that we have to define the geometry of the models and the correct boundary conditions to apply to it. For the FEM calculation, the Young's modulus (E), Poisson's ratio (υ) and the density (ϱ) are needed. The values selected are based on the available published literature (Bird and Kong, 1994; Cai and Wang, 2001; Chery *et al.*, 2001; Lynch

and Richards, 2001; Malservisi *et al.*, 2003; Parsons, 2006; Flesch *et al.* 2007).

Elastic behaviour of crust is assumed for the modelled area and this is justifiable since rheology changes from elastic to viscous at depths greater than 16 km depth in the study area (Fuis and Mooney, 1990). Recent studies of Becken *et al.* (2008) also show that the elastic (seismogenic) crust extends at least up to 12-15 km depth. Realistic boundary conditions have been applied to match the present-day plate kinematics in the Western North America and Pacific boundary.

Model geometry

The model covers the entire California area and consists of 1638 triangular elements and 879 nodes in plane stress condition. There are three types of models: (A) a first model consisting in whole California as a homogeneous one domain, (B) a second model with three domains (Pacific plate, North American plate and San Andreas Fault Zone), and (C) a third model
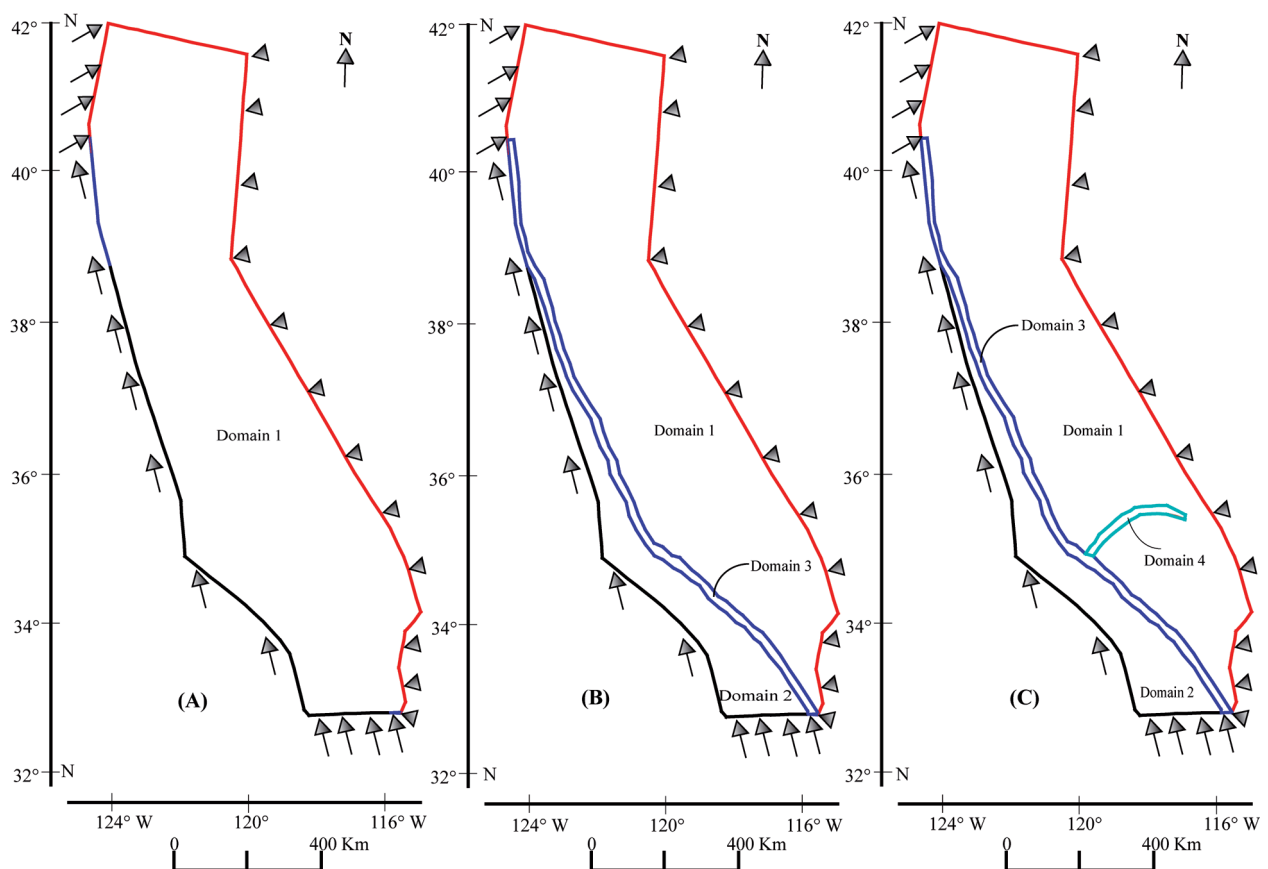
Figure 2. Geometry and boundary condition of: (A) single domain model, (B) three domains model, and (C) four domains model.

with four domains consisting of the Garlock Fault zone as fourth domain and the other three domains being the same as in the second model. The Fault zone boundary is made somewhat zigzag to mimic the actual fault geometry. Obviously, the width of the fault zone is slightly different at different places (Fig. 2).

Boundary condition

The boundary condition imposed represents the present-day plate kinematics of the Pacific plate, remnants of the Farallon plate and North American plate in the Western North America. In all models, the displacement boundary condition is given (Fig. 2). The domain west of the San Andreas Fault is considered as part of the Pacific plate and east of San Andreas is considered as the North American plate. In the model, the Pacific plate is driven by a displacement vector parallel to N34W vector and the North American plate is fixed. Fault-oblique displacement is imposed progressively from 0 m to 250 m, 500 m and 1000 m. In the northeastern portion of the model

after the San Andreas bends offshore to the Mendocino fracture zone (Figs. 1 and 2), oblique convergence boundary condition is imposed, where the Gorda plate and further north the Juan de Fuca plate descend below the North American plate. As the convergent rate of the Gorda plate and the Juan de Fuca plate is less than that of the Pacific plate, only 60% of the displacement rates imposed for the Pacific plate are applied to this boundary along the N50E vector. The northern part of the model is free to move in any direction (Fig. 2).

Rock domain properties

Rock domain properties, geometry, model dimensions and the imposed displacement strongly influence the results of the numerical modelling. Selection of the suitable rock properties for each domain is crucial. In this calculation, the model is highly simplified, so that the properties of the upper crustal rocks are chosen for the calculation. The parameters taken to constrain the rock domain properties are density,
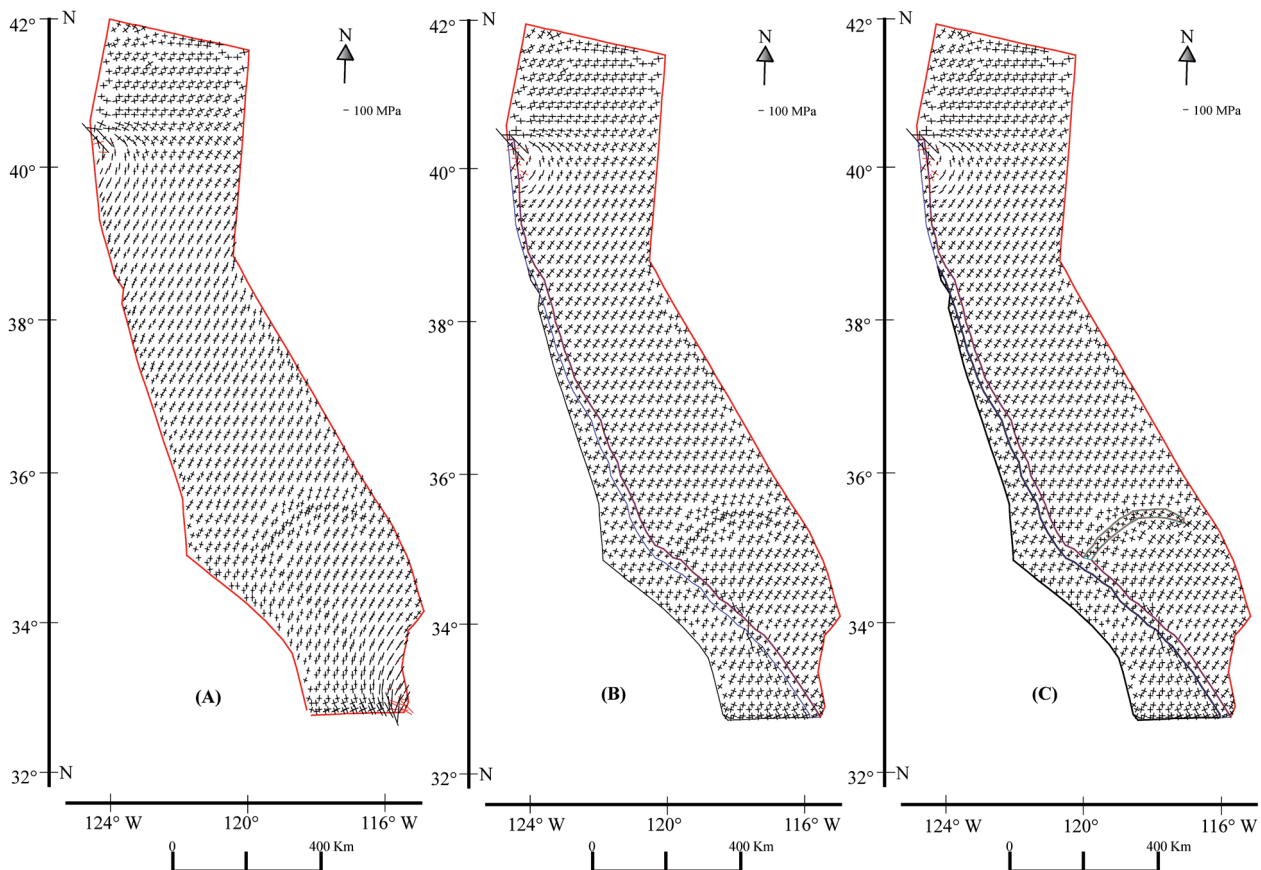
Figure 3. Stress distribution at 250 m displacement for models (A), (B), and (C) respectively; each pair of perpendicular lines represents σ_{Hmax} (long lines) and σ_{Hmin} (short lines) in the stress field, and the red bar shows the tension.
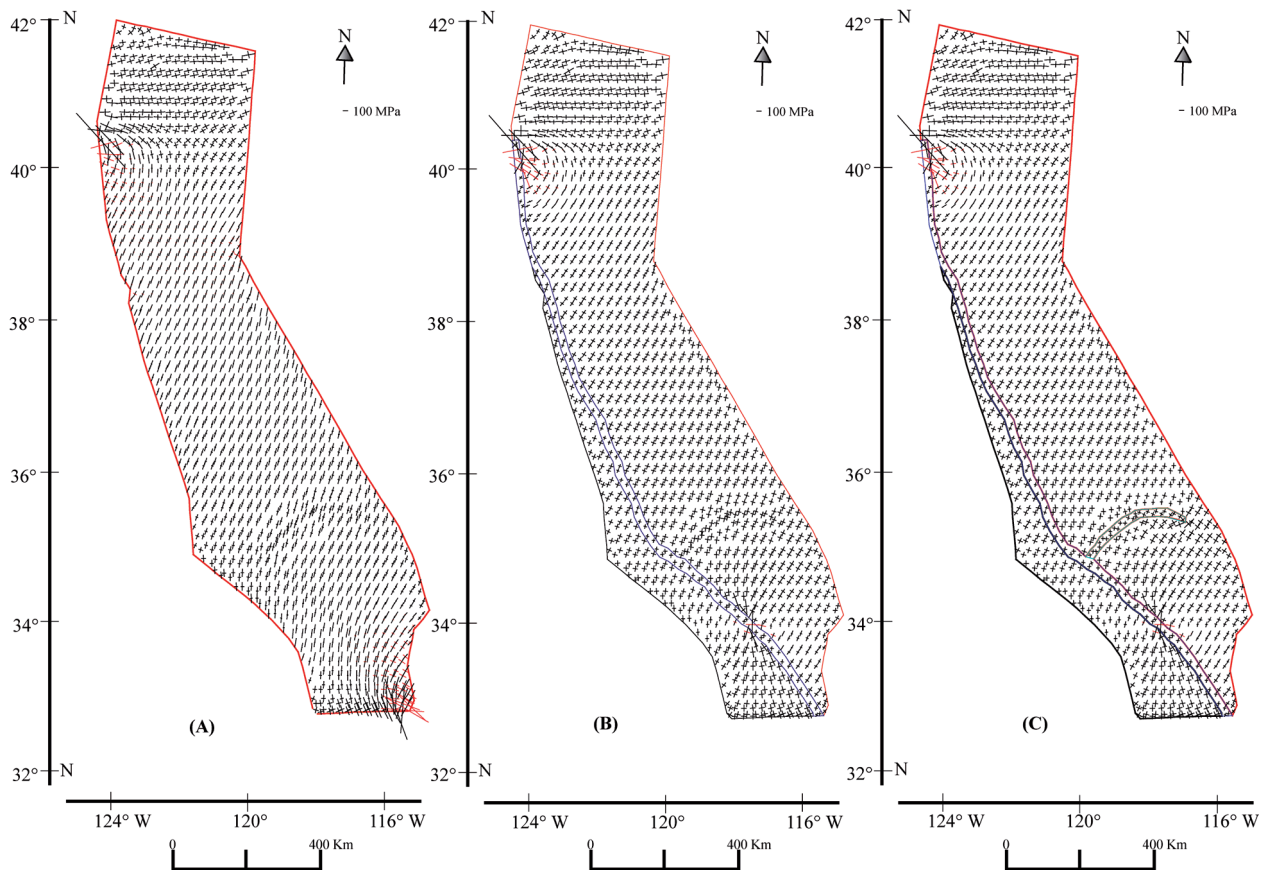
Figure 4. Stress distribution at 500 m displacement for models (A), (B), and (C) respectively; each pair of perpendicular lines represents σ_{Hmax} (long lines) and σ_{Hmin} (short lines) in the stress field, and the red bar shows the tension.

Young's modulus, and Poisson's ratio. The parameters for the rock domains are taken as follows. The Pacific plate and the North American plate are simulated with a Young's modulus of 80 GPa, density of 2800 kg m^{-3} and a Poisson ratio of 0.25. The fault zones are simulated with a Young modulus of 1 GPa, density of 2000 kg m^{-3} and Poisson ratio of 0.25. For all the domains the depth is considered to be 12 km.

Modelling results

As discussed above, the simulation of California is based on a simplified geological map. Three models are created as mentioned above and the general properties of the upper crustal layer are taken to constrain the elastic models. Progressive oblique displacement along the fault is imposed in all models as mentioned already.

Stress field

The stress field for the three models with increasing displacement is shown in figures 3, 4 and 5. Long lines are the maximum horizontal principal stress σ_{Hmax} and the short lines are the minimum horizontal principal stress σ_{Hmin}. As the SAFS is in a transpressional regime, σ_1 is expected to be equal to σ_{Hmax}. The red lines in the models show the tension, while the black lines show the compression. When we consider the one domain model (A), the trend of the maximum horizontal stress is generally NE-SW south of the 40ºN latitude. North of the 40ºN latitude, the trend of the maximum horizontal stress is almost E-W. The boundary between both regions is characterized by few NW-SE and NE-SW stress orientations. The southwestern part south of the 35ºN latitude is characterized by a N-S stress orientation (Figs. 3A, 4A and 5A). The σ_{Hmax} is compressive. A similar pattern of the stress field is observed with increasing displacement boundary condition, but the minimum stress (σ_{Hmin}) with increasing displacement boundary condition becomes tensional and the magnitude of σ_{Hmax} increases. When we consider the three domains model (B) (Figs. 3B, 4B and 5B), the general stress field is similar to that of the one domain model (A), but the magnitude of σ_{Hmin} increases and it mainly becomes compressive, while again the magnitude of the σ_{Hmin} decreases with the increasing dis-
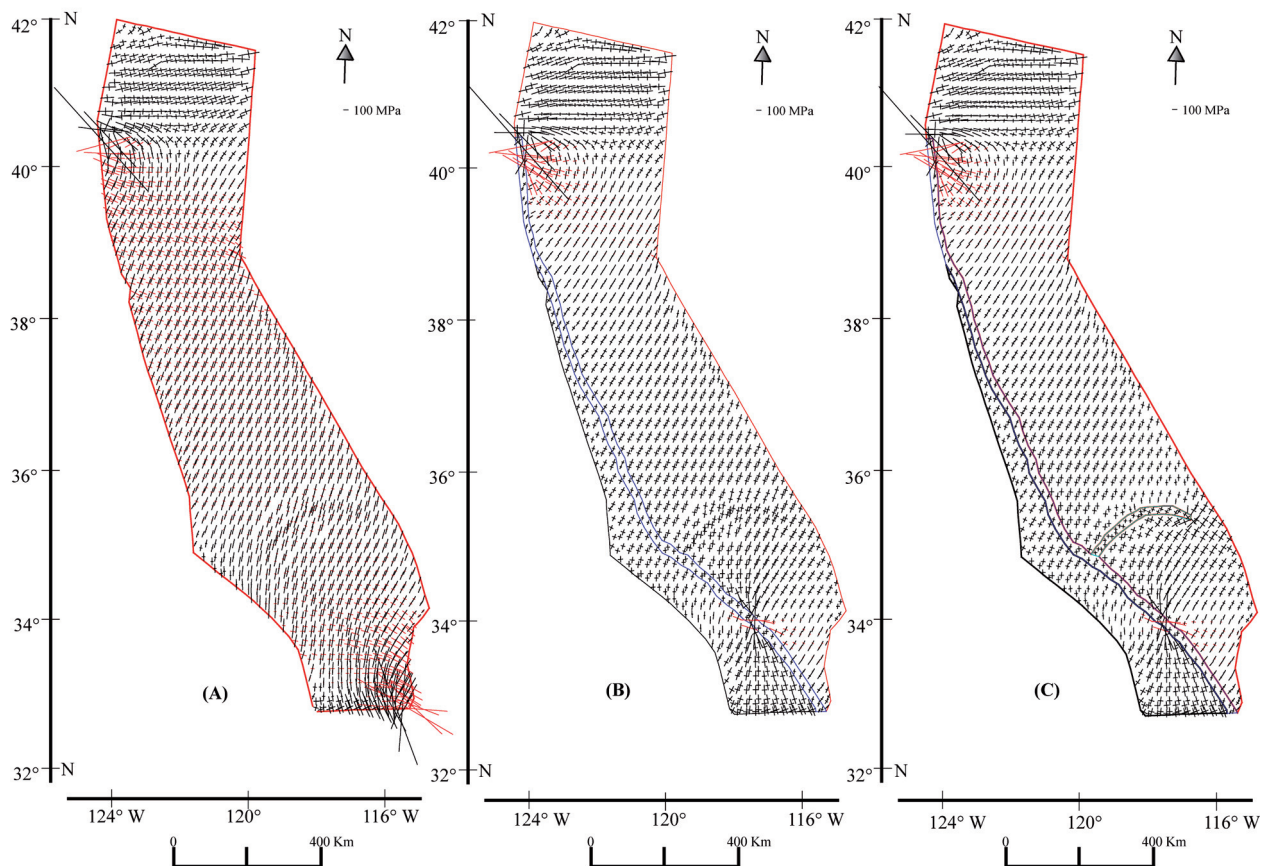
Figure 5. Stress distribution at 1000 m displacement for models (A), (B), and (C) respectively; each pair of perpendicular lines represents σ_{Hmax} (long lines) and σ_{Hmin} (short lines) in the stress field, and the red bar shows the tension.
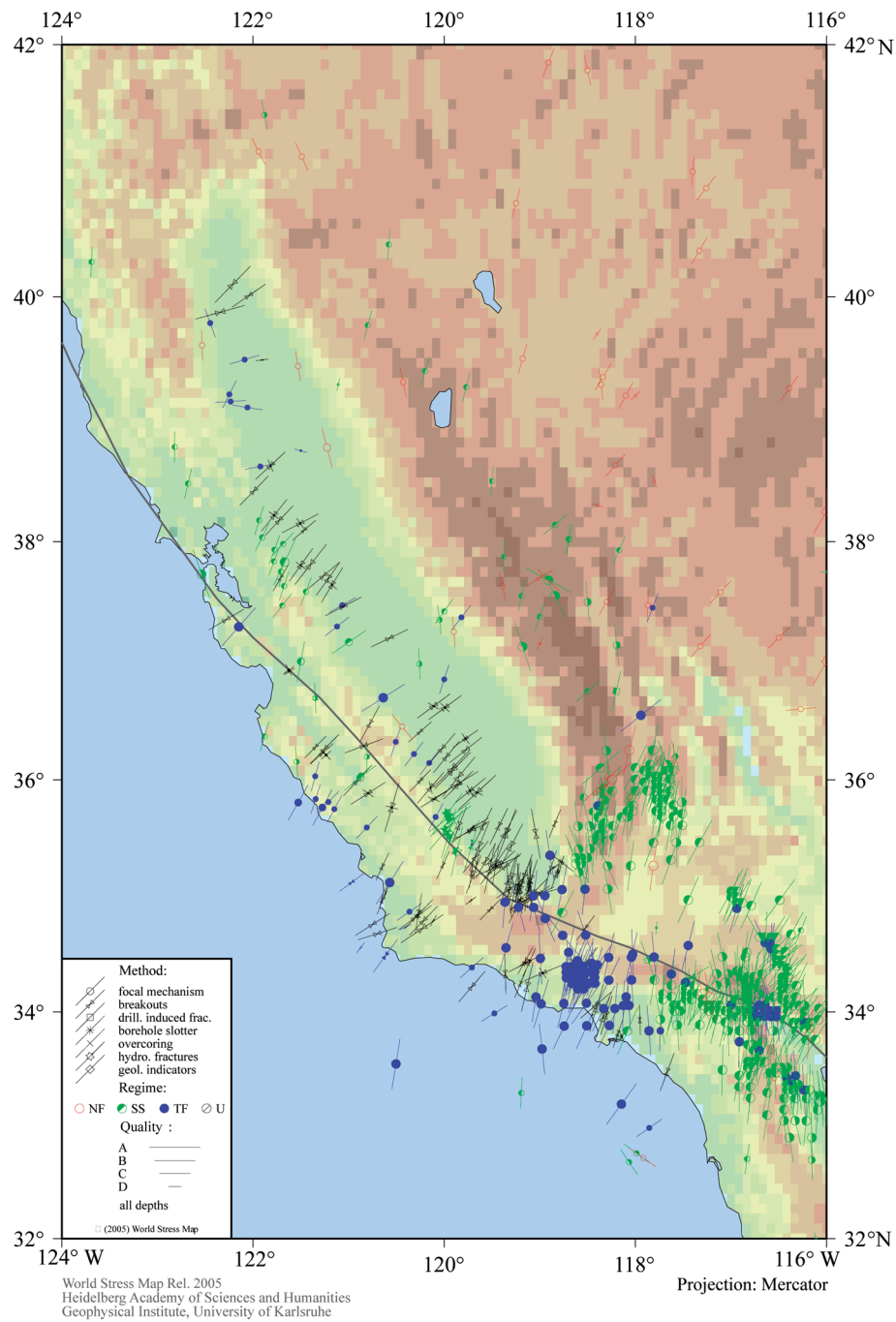
placement boundary condition. South of the latitude of Big Bend near to the SAFS zone, σ_{Hmax} is more oblique to the strike of the SAFS but SE of the Garlock Fault some σ_{Hmax} are perpendicular to the SAFS strike (Figs. 3B, 4B and 5B). There is no such variation in the stress field in the four domains model (C) with the Garlock Fault. It is similar to the three domains model (B) but the trend of the stress just north of the Garlock Fault is now N-S.

The calculated stress fields in our models are in good agreement with the world stress map (Fig. 6). Both the regional stress field and σ_{Hmax} orientation in all three models are similar, but models (B) and (C) show a stress perturbation due to SAFS Big Bend and Garlock Fault.

Velocity vector

Velocity vectors for the three models with increasing displacements are shown in figures 7, 8 and 9. In these figures, the arrow shows the direction of motion, while the length of the arrow is the magni-

tude. The general trend of the displacement is towards N34W south of 40°N latitude, but between 40°N and 42°N latitude the displacement is towards N50E direction. Increasing the displacement boundary condition causes only an increase in magnitude of the displacement vector (Figs. 7A, 8A and 9A). When we consider the three domains model (Figs. 7B, 8B and 9B), the general trend is the same as in the one domain model (A), but SE of the Big Bend and south of the Garlock Fault the displacement vector is rotated towards north. Increasing displacement boundary condition increases only the magnitude of the displacement (Figs. 7B, 8B and 9B). When we consider the four domains model (C), the general trend of the displacement vector is the same as in the three domains model (B) and the magnitude of the displacement vector increases with increasing displacement. Nevertheless, in the Garlock Fault zone, north of the fault zone the displacement is towards NW and south of the fault zone the displacement is towards NE with high magnitude. Therefore, the Garlock Fault is simulated as a left-lateral strike slip fault in our model. This can be visualized in the models with

Figure 6. Orientation of maximum horizontal stress observed in and around the modeled area (after Reinecker *et al.*, 2005).

increasing displacement boundary condition (Figs. 7C, 8C and 9C).

Our calculated displacement vectors are comparable in terms of the regional sense of movement with the velocity model (Flesch *et al.*, 2007) and GPS velocity (Flesch *et al.*, 2007 and references therein), and in our models (B and C) the Big Bend of the SAFS and Garlock Fault have local effects on the displacement vector.

Discussion

Model setup and limitations

Although in nature there are vertical and lateral variations in the rheology, and the material types are inhomogeneous, the models are constructed considering simplified homogeneous and isotropic domain properties. Elastic rheology is taken for modelling purposes and this is justifiable because 12 km is the seismogenic
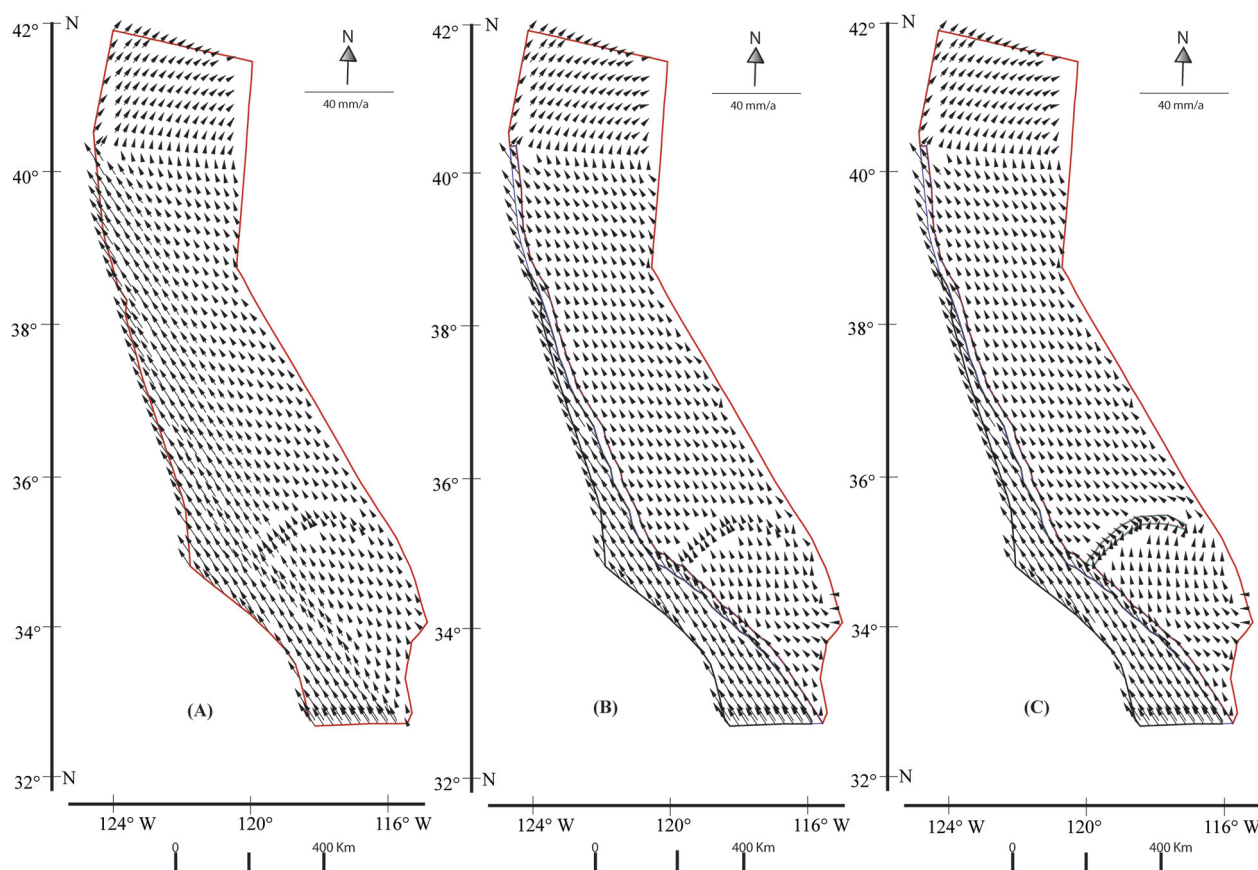
Figure 7. Velocity vectors at 250 m displacement for models (A), (B), and (C) respectively.

depth in the California area. General parameters for the rock domain are based on the published literature as defined above. There are many parallel and subparallel strands of the SAFS but we consider only the biggest and main strand, namely the Garlock Fault. Since the political boundary of the California State is taken as the model area boundary, there may be some boundary effects due to model boundary geometry, but it seems that this effect is very small. As this modelling only considers the elastic thickness of the crust, the effect of the plastic layer below the SAFS and the viscous layer at depth may significantly deviate the results.

*Maximum compressive horizontal stress (σ_{Hmax})*

Many methods like borehole breakouts, focal mechanisms inversions, drill induced fractures etc., are used for the calculation of the stress fields, especially the maximum compressive horizontal stress (σ_{Hmax}). Orientations of the maximum and minimum horizontal stresses are calculated by various authors to show the differential stress in the seismogenic depth of California (Parsons, 2006). Most of the measured stresses shown in the world stress map (Fig. 6) and modelled data

(Parsons, 2006) show that the orientation of the maximum horizontal stress is nearly orthogonal to the SAFS along most of its length. The measured maximum principal stress direction (σ_{Hmax}) within 20 km from the fault trace on both sides of the fault shows fault-oblique compression and farther than this distance shows fault-perpendicular compression. In our models, the stress orientations are more or less homogeneously oriented showing fault-oblique compression throughout California and the deviation from this pattern in southern California is due to Big Bend and Garlock Fault. Similar results were also obtained by Li and Liu (2006).

Conclusions

The results of this study led us to the following conclusions: (1) since the calculated stress field is in good agreement with other measured data (borehole breakouts, focal mechanisms inversions and drill-induced fractures) and the calculated displacement vectors are in good agreement with measured GPS velocity, this implies that our imposed boundary condition is able to simulate the present-day tectonic setting. (2) Increasing displacement boundary condition (e.g. Fig. 5A) can produce tension-
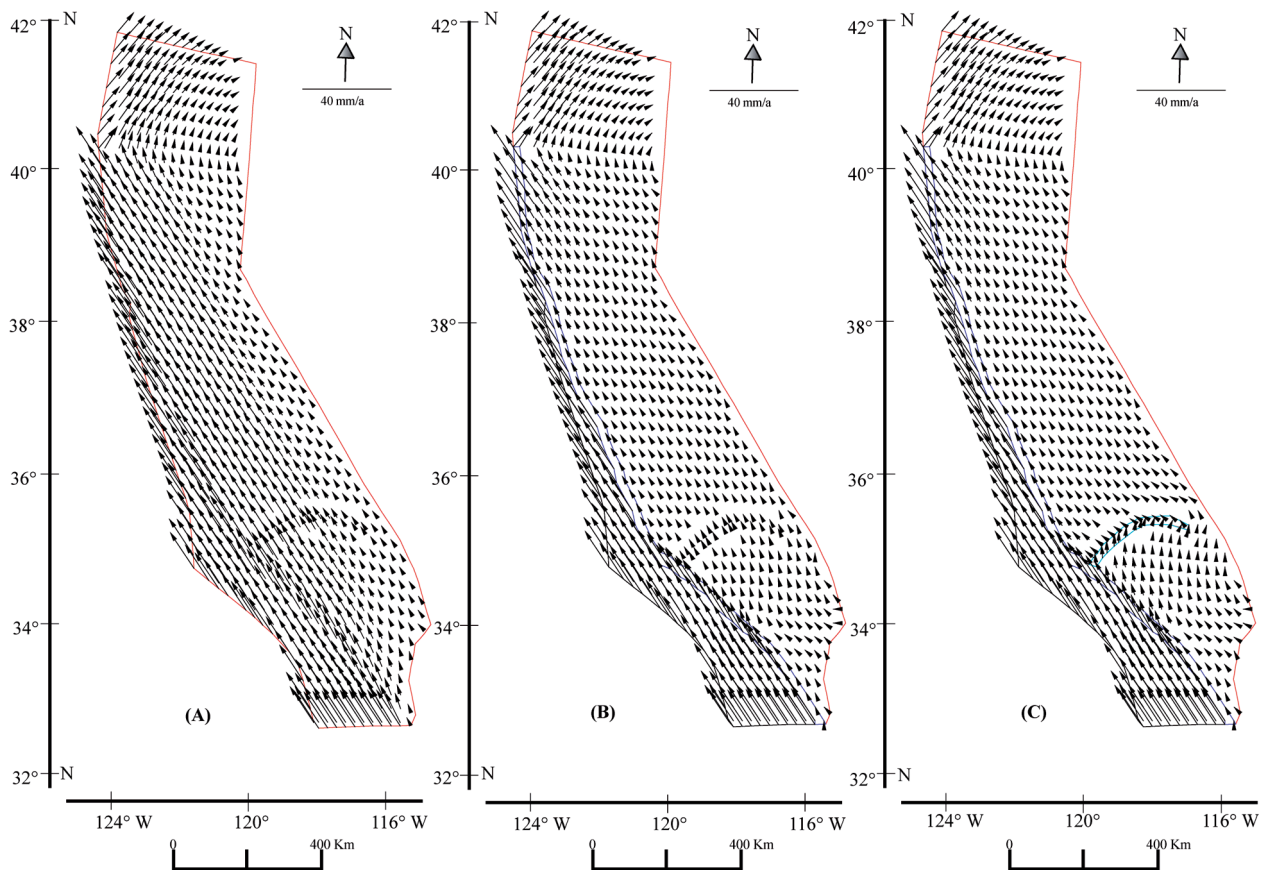
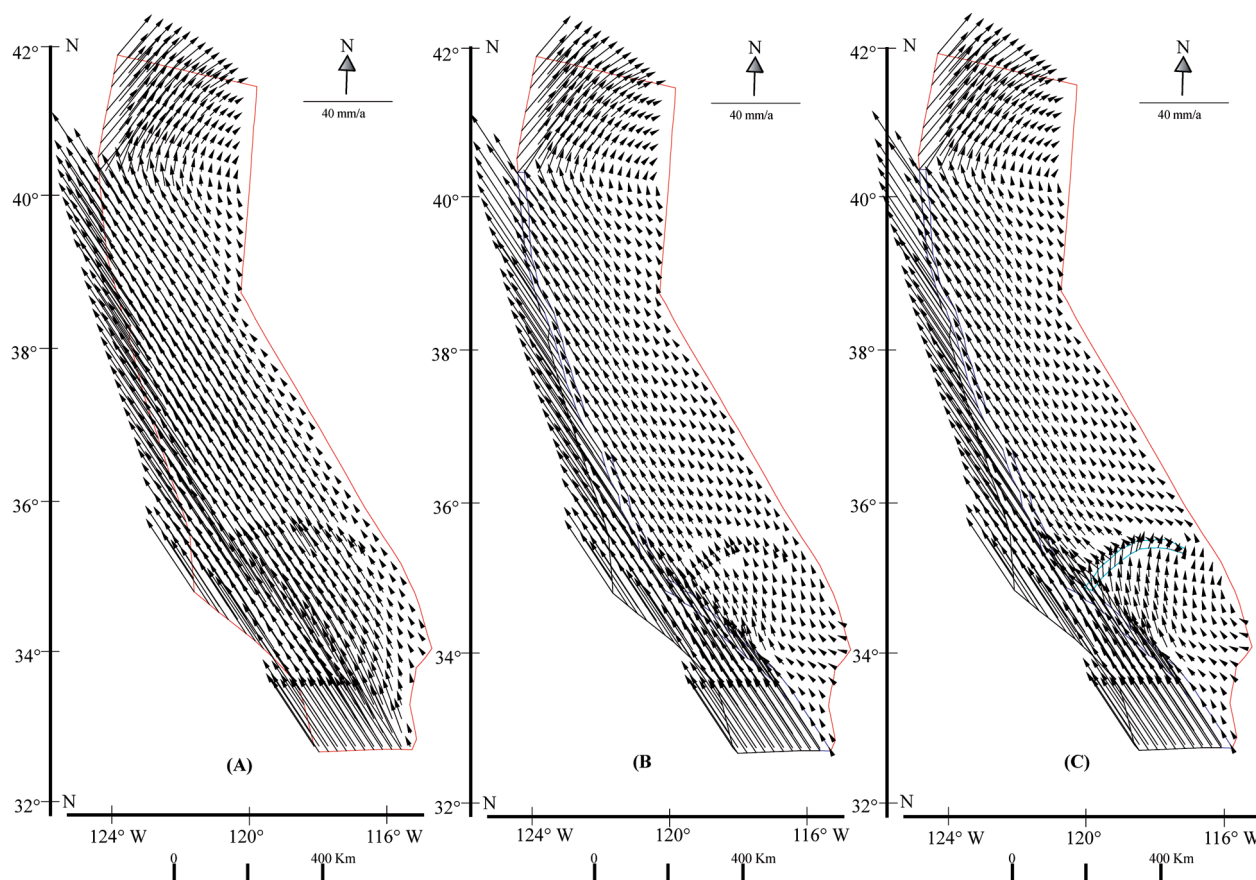**Figure 8.** Velocity vectors at 500 m displacement for models (A), (B), and (C) respectively.

al stress σ_{Hmin}, but σ_{Hmax} is usually compressive. (3) Generally, σ_{Hmax} is oblique to the SAFS. (4) The Big Bend of the SAFS and Garlock Fault has a local effect on the stress field as well as on the displacement vector which may have significant impact on fault slip, stress, and hence deformation in the surrounding region. Seismicity in southern California may be influenced by the combined effect of the Big Bend and Garlock Fault.

References

ARGUS, D. F. and GORDON R. G. (2001): Present tectonic motion across the Coast Ranges and the San Andreas fault system in central California. *Geol. Soc. Am. Bull.,* 113: 1580-1592.

ATWATER, T. (1970): Implications of plate tectonics for the Cenozoic tectonic evolution of western North America. *Geol. Soc. Am. Bull.,* 81: 3513-3635.

BECKEN, M., RITTER, O., PARK, S. K., BEDROSIAN, P. A., WECKMANN, U. and WEBER, M. (2008): A deep crustal fluid channel into the San Andreas Fault system near Parkfield, California. *Geophys. J. Int.,* 173: 718-732. doi: 10.1111/j.1365-246X.2008.03754.x.

BIRD P. and KONG X. (1994): Computer simulations of California tectonics confirm very low strength of major fault. *Geol. Soc. Am. Bull.,* 106: 159-174.

CAI, Y. and WANG C. Y. (2001): Testing fault models with numerical simulation: example from central California. *Tectonophysics,* 343: 233-238.

CHERY J., ZOBACK M. D. and HASSANI R. (2001): An integrated mechanical model of the San Andreas fault in central and northern California. *J. Geophys. Res.,* 106: 22 051-22 066.

D'ALESSIO, M. A., JOHANSON, I. A., BÜRGMANN, R., SCHMIDT, D. A. and MURRAY, M. H. (2005): Slicing up the San Francisco Bay Area: Block kinematics and fault slip rate from GPS-derived surface velocities. *J. Geophys. Res.,* 110 (B06403): 1-19. doi: 10.1029/2004JB003496.

Figure 9. Velocity vectors at 1000 m displacement for models (A), (B), and (C) respectively.

DEMETS, C., GORDON, R. G., ARGUS, D. F. and STEIN, S. (1994): Effects of recent revisions to the geomagnetic reversal time scale on estimates of current plate motions. *Geophys. Res. Lett.*, 21: 2191-2194.

FLESCH, L. M., HOLT, W. E., HAINES, A. J., WEN, L. and SHEN-TU B. (2007): The dynamics of western North America: stress magnitudes and the relative role of gravitational potential energy, plate interaction at the boundary and basal tractions. *Geophys. J. Int.,* 169: 866-896. doi: 10.1111/j.1365-246X.2007.03274.x.

FUIS, G. S. and MOONEY, W. D. (1990): Lithospheric structure and tectonics from seismic-refraction and other data. *In*: R. E. WALLACE (ed): *The San Andreas Fault System.* USGS Professional Paper, 1515: 207-236.

HAYASHI D. (2008): Theoretical basis of FE simulation software package. *Bulletin of Faculty of Science University of the Ryukyus,* 85: 81-95. http://ir.lib.u-ryukyu.ac.jp/

IRWIN, W. P. (1990): Geology and Plate-Tectonic Development. *In*: R. E. WALLACE (ed): *The San Andreas Fault System.* USGS Professional Paper, 1515: 61-80.

LI, Q. and LIU, M. (2006): Geometrical impact of the San Andreas Fault on Stress and Seismicity in California. *Geophys. Res. Lett.,* 33 (L08302): 1-4. doi: 1029/2005GL025661.

LYNCH, J. C. and RICHARDS, M. A. (2001): Finite elements models of the stress orientations in well-developed strike-slip fault zones: Implications for the distribution for lower crustal strain. *J. Geophys. Res.*, 106: 26 707-26 729.

MALSERVISI, R., GANS C. and FURLONG K. P. (2003): Numerical modeling of strike-slip creeping faults and implications for the Heyward fault, California. *Tectonophysics,* 361: 121-137.

MINSTER, J. B. and JORDAN, T. H. (1978): Present-day plate motions. *J. Geophys. Res.,* 83: 5331-6354.

NOSON, L. L., QAMAR, A. and THORSEN, G. W. (1988): Washington State Earthquake Hazards. Washington State Department of Natural Resources, Washington Division of Geology and Earth Resources, Information Circular 85. http://www.pnsn.org/INFO_GENERAL/NQT/welcome.html

PARSONS, T. (2006): Tectonic stressing in California modeled from GPS observations. *J. Geophys. Res.*, 111(B03407): 1-16. doi: 10.1029/2005JB003946.

REINECKER, J., HEIDBACH, O., TINGAY, M., SPERNER, B. and MÜLLER, B. (2005): The 2005 release of the World Stress Map. www.world-stress-map.org

SAVAGE, J. C., GAN, W. PRESCOTT, W. H. and SVARC J. L. (2004): Strain accumulation across the Coast Ranges at the latitude of San

Francisco, 1994-2000. *J. Geophys. Res.*, 109(B03413): 1-11. doi: 10.1029/2003JB002612.

Swanson D. A., Cameron K. A., Evarts R. C., Pringle P. T. and Vance J. A. (1989): Cenozoic Volcanism in the Cascade Range and Columbia Plateau, Southern Washington, and Northernmost Oregon. *AGU Field Trip Guidebook,* T106.http://vulcan.wr.usgs.gov/Volcanoes/PacificNW/AGUT10 6/hood.html#mounthood

Wallace, R. E. (1990): General Features and Geomorphic Expression. *In*: R. E. Wallace (ed): *The San Andreas Fault System.* USGS Professional Paper, 1515: 3-21.

Wood, C. A. and Kienle, J. (1990): *Volcanoes of North America: U.S. and Canada.* Cambridge University Press, 354 pp. ISBN 052143811X, 9780521438117.